Energy & Environmental Science

ROYAL SOCIETY OF CHEMISTRY

PAPER

View Article Online
View Journal | View Issue

Check for updates

Cite this: *Energy Environ. Sci.*, 2025, **18**, 3296

Fluorinated-oligomeric ionic liquids for high-performance wide-temperature solid zinc batteries†

Ze Chen,[a] Tong Liu,[b] Zhiquan Wei,[c] Yiqiao Wang,[c] Ao Chen,[c] Zhaodong Huang,[c] Duanyun Cao,*[b] Nan Li *[c] and Chunyi Zhi *[cde]

Zn-based solid polymer electrolytes (SPEs) hold immense potential for developing high-performance and safe zinc ion batteries (ZIBs) that can operate effectively even at high temperatures. However, typical plasticizers like ionic liquids (ILs) exhibit limitations regarding Zn^{2+} ion transport and compatibility with the polymer matrix, causing a low Zn^{2+} transference number ($t_{Zn^{2+}}$) and serious phase separation in SPEs. In this study, we develop a novel fluorinated IL (F-IL) plasticizer containing an imidazole cation with a fluoro alkyl substituent as an extended side chain for zinc-based SPEs. This innovative imidazole cation effectively modifies the Zn^{2+} solvation structure. It significantly enhances the compatibility between ILs and the polymer matrix, enabling fast Zn^{2+} ion transport (with a notable $t_{Zn^{2+}}$ of 0.46 and high ionic conductivity of 2.8×10^{-3} S cm^{-1}) when incorporated in SPEs. Using the F-ILs-based SPE, we achieve dendrite-free Zn plating/stripping cycling over 2000 h, even at high temperatures. A Zn‖Cl4Q battery assembled with the designed SPE outperforms other solid ZIBs, demonstrating a wide working temperature range (−15 °C to 120 °C) and a long cycling life (capacity retention 70.9% after 2000 cycles at 90 °C). In addition, the pouch cell exhibits a remarkable shelf life (90 days) and a low self-discharge rate (capacity loss of 0.09% per day) at 60 °C, thanks to the high thermal and chemical stability of the SPE during operation. The F-IL-based SPE, with its advanced ion transport structure, provides solid ZIBs with significant performance improvement, high safety, and enduring durability.

Received 4th November 2024,
Accepted 19th February 2025

DOI: 10.1039/d4ee05153j

rsc.li/ees

Open Access Article. Published on 20 February 2025. Downloaded on 5/22/2025 12:07:16 AM.
This article is licensed under a Creative Commons Attribution-NonCommercial 3.0 Unported Licence.

Broader context

Aqueous zinc ion batteries (ZIBs) are prevented from practical applications at high temperature due to the poor thermal stability of water and the severe side reactions of electrodes. Solid ZIBs hold great promise for wide-temperature application with maintained safety and stability. In the present work, a fluorinated ionic liquid (IL) plasticizer containing an imidazole cation with a fluoro alkyl substituent as an extended side chain was developed as a zinc-based solid electrolyte. This innovative imidazole cation effectively modifies the Zn^{2+} solvation structure. It significantly enhances the compatibility between the IL and the polymer matrix, enabling fast Zn^{2+} ion transport. Dendrite-free Zn plating/stripping cycling over 2000 h with low polarization potentials, even at high temperatures, is achieved. Furthermore, the full cell could work properly at a wide working temperature range (−15 °C to 120 °C) with a remarkable shelf life (90 days) and a low self-discharge rate at 60 °C. This discovery is an exemplary effort and provides solid ZIBs with significant performance improvement, high safety, and enduring durability.

[a] *School of Interdisciplinary Studies, Lingnan University, 8 Castle Peak Road, Tuen Mun, Hong Kong, China*
[b] *Beijing Key Laboratory of Environmental Science and Engineering, School of Materials Science and Engineering, Beijing Institute of Technology, Beijing, 100081, China. E-mail: dycao@bit.edu.cn*
[c] *Department of Materials Science and Engineering, City University of Hong Kong, 83 Tat Chee Avenue, Kowloon, Hong Kong, 999077, China. E-mail: nanli75@cityu.edu.hk, cy.zhi@cityu.edu.hk*
[d] *Hong Kong Center for Cerebro-Cardiovascular Health Engineering (COCHE), Shatin, NT, HKSAR, China*
[e] *Hong Kong Institute for Clean Energy, City University of Hong Kong, Kowloon, 999077, Hong Kong*

† Electronic supplementary information (ESI) available. See DOI: https://doi.org/10.1039/d4ee05153j

Introduction

Aqueous zinc ion batteries (ZIBs) have recently garnered significant interest due to the high theoretical capacity (820 mA h g^{-1}) and low redox potential (−0.76 V *vs.* standard hydrogen electrode) of the Zn anode, coupled with the exceptional safety offered by their aqueous nature.[1–3] However, the advancement of aqueous ZIBs is hampered by concomitant issues of aqueous electrolytes, including generation of Zn dendrites, parasitic hydrogen evolution reaction (HER), corrosion, passivation, and narrow working temperature.[4–6] Several alternative electrolytes, such as "water-in-salt" electrolyte,[7]

This journal is © The Royal Society of Chemistry 2025

Open Access Article. Published on 20 February 2025. Downloaded on 5/22/2025 12:07:16 AM.
This article is licensed under a Creative Commons Attribution-NonCommercial 3.0 Unported Licence.

hydrate-melt electrolyte,[8] organic electrolyte,[9] and hydrogel electrolyte,[10] have been suggested to address these issues; however, these electrolytes, at best, can only alleviate but not completely eradicate the aforementioned problems, whilst some of them also exhibit drawbacks like high cost and tedious preparation.[11,12]

Solid polymer electrolytes (SPEs) offer an exciting solution for addressing the complicated challenges in ZIBs due to their water-free nature, high thermal and electrochemical stability, exceptional safety, and wide operation temperature window (Fig. 1a).[5,13] However, Zn^{2+} ion transport in SPEs overly relies on the random motion of the polymer chains, which shows sluggish dynamics, leading to poor ionic conductivity ($\sim 10^{-5}$ to 10^{-7} S cm^{-1} at 25 °C).[14] The conventional SPEs, composed of zinc salts and a polymer matrix, involve the movement of both anions and cations, causing salt concentration gradients and cell polarization with a low Zn^{2+} transference number ($t_{Zn^{2+}}$) (mostly below 0.4).[15] The simultaneous achievement of high ionic conductivity and high $t_{Zn^{2+}}$ represents a significant challenge for the further advancement of Zn-based SPEs.[16,17]

Incorporating ionic liquids (ILs) as plasticizers in SPEs is a promising approach to improve the ionic conductivity by increasing the segmental mobility of polymer chains.[18,19] ILs own various advantages, such as ultra-low vapor pressure, broad electrochemical stability window (ESW), high thermal and chemical stability, and nonflammability.[20–22] However, a significant challenge arises from the poor compatibility between ILs and the polymer matrix (Fig. 1bi), which can be attributed to the difference in polarity, viscosity, molecular size, and structure between ILs and the polymer matrix. Additionally, the strong ionic interactions in ionic liquids can impede effective interaction with the polymer chains. This incompatibility often results in severe macro-phase separation, which obstructs ion transfer at the interface and compromises phase stability.[23,24] Moreover, the inclusion of ILs can "dilute" Zn^{2+} conductive paths in SPEs and, in some instances, increase Zn^{2+}-anion interaction, leading to slow Zn^{2+} ion migration;[19] meanwhile, the addition of IL ions that do not contribute to Zn^{2+} ion transport can also reduce $t_{Zn^{2+}}$. Both can impede Zn^{2+} ion transport and limit potential performance improvements when employing these SPEs in ZIBs.[25] Therefore, decoupling Zn^{2+} ion transport from the segmental mobility of polymer chains and enhancing the compatibility between ILs and the polymer matrix are of significant importance to promote the electrochemical performance of SPE-based zinc batteries.

In this study, we synthesized a novel fluorinated IL (F-IL) plasticizer, 1-ethyl-3-fluoro alkyl imidazolium bis(trifluoromethylsulfonyl)imide with a median fluoro alkyl chain (denoted as MIMTFSI). The imidazole cation with a fluorinated substitute significantly enhanced Zn^{2+} ion solvation and the compatibility between the F-IL and the polymer matrix due to the improved polarity of ILs and the interaction like van der Waals forces or hydrogen bonding between the two components, contributing to accelerated Zn^{2+} ion transport in ZIBs (with a high ionic conductivity of 2.8×10^{-3} S cm^{-1} and a notable $t_{Zn^{2+}}$ of 0.46). Owing to the high thermal stability of the F-IL-based SPE, highly reversible Zn plating/stripping cycling was achieved, completely eradicating Zn dendrite and HER issues, even at elevated temperatures. Leveraging these benefits, we constructed a solid Zn‖Cl4Q battery with a wide operating temperature range, which demonstrated superior electrochemical performance and cycling life compared to other solid ZIBs, along with an exceptional shelf life (90 days) and a low self-discharge rate (capacity loss of 0.09% per day) at 60 °C.

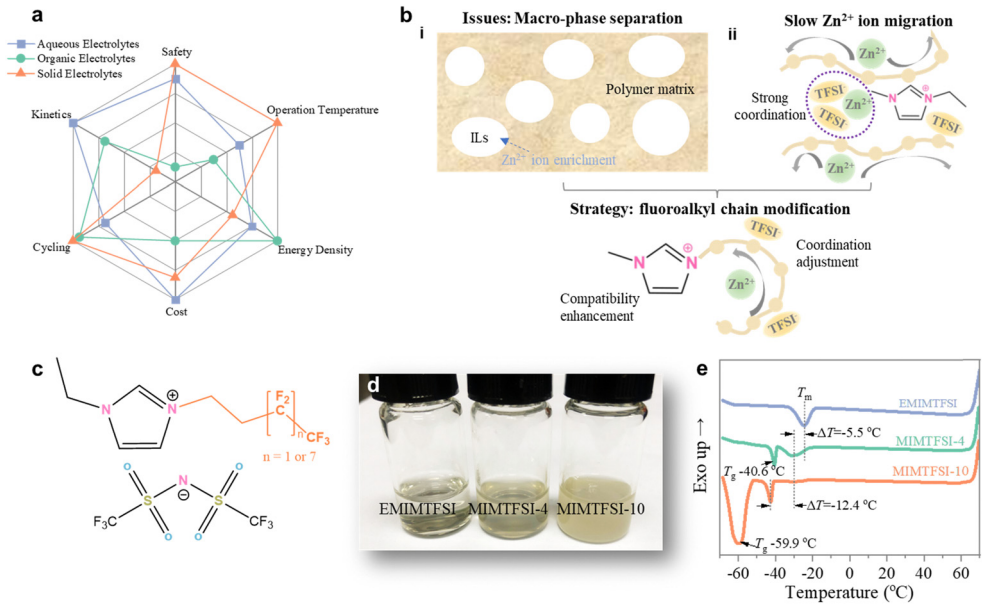

Fig. 1 Design strategy and characteristics of F-IL plasticizers. (a) Comparison of various electrolytes for ZIBs; (b) illustration of the accelerated ion conduction by F-IL plasticizers, where F-ILs not only enhance the compatibility with the polymer matrix but also improve the Zn^{2+} ion solvation structure; (c) chemical structures of as-synthesized F-ILs; (d) optical pictures of the ILs; (e) DSC test of the ILs.

Open Access Article. Published on 20 February 2025. Downloaded on 5/22/2025 12:07:16 AM.
This article is licensed under a Creative Commons Attribution-NonCommercial 3.0 Unported Licence.

Results and discussion

Synthesis and characteristics of the F-ILs

Compared to traditional imidazole-based ILs, the imidazole cation with a fluorinated substitute shows great potential for enhancing Zn^{2+} ion solvation and improving compatibility with the polymer matrix. This could lead to faster Zn^{2+} ion transport in ZIBs (Fig. 1bii and iii). The F-ILs were synthesized by reacting 1-ethylimidazole and iodoalkane at 90 °C for 3 days (Fig. S1, ESI†). Subsequently, the F-ILs were isolated through an anion exchange with bis(trifluoromethylsulfonyl)imide ($TFSI^-$). To illustrate the influence of fluorinated side chains, we used commercial 1-ethyl-3-methylimidazolium bis(trifluoromethylsulfonyl)imide (EMIMTFSI) without fluorinated side chains as a control sample and synthesized two F-ILs, 1,1,1,2,2-pentafluoro-4-iodobutane and 1-iodo-1*H*,1*H*,2*H*,2*H*-perfluorodecane (denoted as MIMTFSI-4 and MINTFSI-10), with different fluorinated side chains (Fig. 1c).

The chemical structures of the two F-ILs are validated by the ^{1}H-NMR spectra (Fig. S2 and S3, ESI†). As illustrated in Fig. 1d, the ILs retain their liquid feature despite the transparency gradually decreasing with the propagation of the side chains. The glass transition temperature (T_g) (−40.6 °C for MIMTFSI-4 and −59.9 °C for MIMTFSI-10) obtained from differential scanning calorimetry (DSC) measurements indicates successful synthesis of F-ILs (Fig. 1e). Additionally, MIMTFSI-10 demonstrates the lowest melting temperature (T_m) at −42.5 °C, highlighting its potential as a wide-temperature electrolyte additive.[26]

Ion conduction mechanism of the F-ILs with zinc salt

Prior to fabricating SPE membranes, we prepared liquid binary electrolytes composed of 1 M $Zn(TFSI)_2$ in ILs (namely $Zn(TFSI)_2$/EMIMTFSI, $Zn(TFSI)_2$/MIMTFSI-4, and $Zn(TFSI)_2$/MIMTFSI-10), to unveil the coordination process between ILs and Zn^{2+} ions. Raman spectroscopy was utilized to examine Zn^{2+} ion solvation in TFSI-based electrolytes regarding the sensitive Raman bands of $TFSI^-$ for ionic coordination analysis, *i.e.*, bands at ∼749 cm^{-1} and ∼742 cm^{-1} corresponding to $TFSI^-$ ions coordinated to Zn^{2+} and "free" (uncoordinated) $TFSI^-$, respectively (Fig. S4, ESI†).[27] Specifically, the area ratio of the coordinated $TFSI^-$ peak to the sum of two peaks allows quantification of the amount of $TFSI^-$ coordinated to Zn^{2+} and derivation of the number of coordinated $TFSI^-$ per Zn^{2+} solvation shell.[19] The results reveal that only a small fraction (∼9%) of $TFSI^-$ ions coordinate to Zn^{2+} ions in $Zn(TFSI)_2$/MIMTFSI-10 (Fig. S4, ESI†), in contrast to ∼50% of coordinated $TFSI^-$ in $Zn(TFSI)_2$/EMIMTFSI. As depicted in Fig. 2a, the number of coordinated $TFSI^-$ anions per Zn^{2+} solvation shell is derived to be approximately two in $Zn(TFSI)_2$/EMIMTFSI, but significantly decreases to 0.39 in $Zn(TFSI)_2$/MIMTFSI-10, indicating that most Zn^{2+} ions lack $TFSI^-$ in their solvation spheres (with only 9% coordinated $TFSI^-$ in the $Zn(TFSI)_2$/MIMTFSI-10 electrolyte). A weakened interaction between Zn^{2+} and $TFSI^-$ with the propagation of fluorinated side chains is indicated by the shift of the vibration stretching band of S–N–S in $TFSI^-$ to a higher wavenumber (Fig. S5, ESI†), probably attributed to the change in Zn^{2+} solvation shell. Such a phenomenon may be partly attributed to the high electronegativity of fluorine atoms, which imparts a partial negative charge to the fluoroalkyl chain and creates a dipole. This dipole can interact with positively charged Zn^{2+} ions through dipole–ion interactions. Additionally, the presence of multiple fluorine atoms also slightly enhances the polarizability of the fluoroalkyl chain, further strengthening these electrostatic

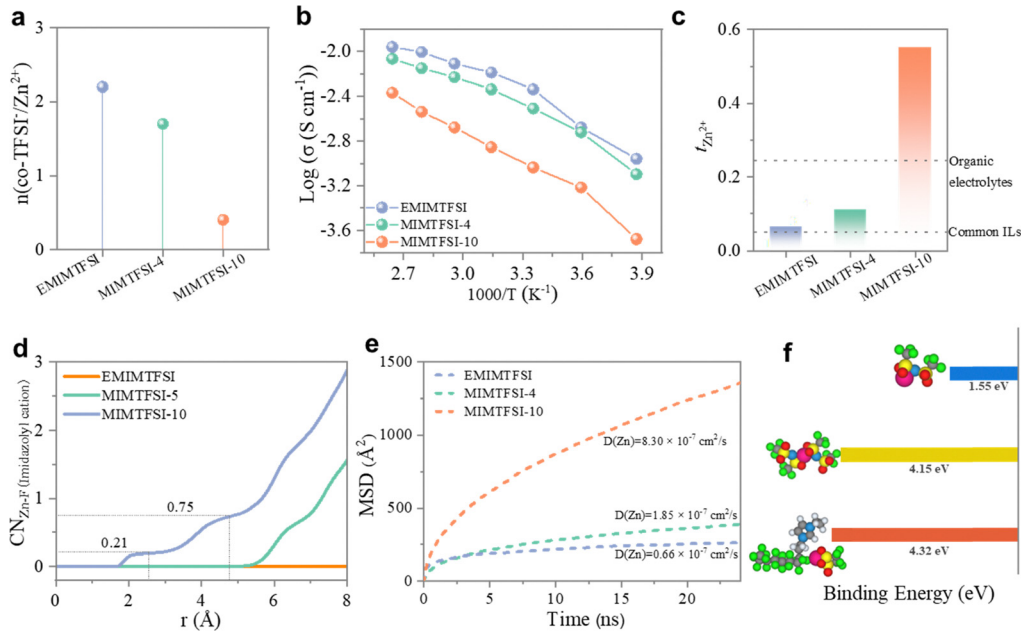

Fig. 2 Investigations into the ion conduction mechanism of the F-ILs with zinc salt. (a) Calculated average number of $TFSI^-$ ions per Zn^{2+} coordination sphere; (b) Arrhenius plots of ionic conductivity of the $Zn(TFSI)_2$/ILs electrolytes in a wide temperature range from −15 °C to 105 °C; (c) $t_{Zn^{2+}}$ of the $Zn(TFSI)_2$/ILs electrolytes at room temperature; (d) RDF of Zn^{2+} in the $Zn(TFSI)_2$/ILs electrolytes; (e) MSD curves of the $Zn(TFSI)_2$/ILs electrolytes; (f) calculated binding energy of various solvation structures in $Zn(TFSI)_2$/MIMTFSI-10.

 This journal is © The Royal Society of Chemistry 2025

Open Access Article. Published on 20 February 2025. Downloaded on 5/22/2025 12:07:16 AM.
This article is licensed under a Creative Commons Attribution-NonCommercial 3.0 Unported Licence.

interactions. These results suggest that most Zn^{2+} ions are fully solvated by the fluorinated side chain.

We subsequently investigated the ionic conductivity of the $Zn(TFSI)_2$/IL electrolytes over a wide temperature range from −15 °C to 105 °C (Fig. 2b), which exhibits a gradual increase with rising temperature, a trend attributable to enhanced molecular dynamics at higher temperatures.[18] The ionic conductivity at room temperature reaches 4.6×10^{-3} S cm^{-1} ($Zn(TFSI)_2$/EMIMTFSI), 3.1×10^{-3} S cm^{-1} ($Zn(TFSI)_2$/MIMTFSI-4), and 9.2×10^{-4} S cm^{-1} ($Zn(TFSI)_2$/MIMTFSI-10), respectively. The slightly lower ionic conductivity of $Zn(TFSI)_2$/MIMTFSI-10 might result from reduced dynamics due to the longer fluorinated side chain.[28] Despite this, a high $t_{Zn^{2+}}$ of up to 0.55 is achieved in $Zn(TFSI)_2$/MIMTFSI-10 (Fig. 2c), significantly exceeding that of $Zn(TFSI)_2$/EMIMTFSI (0.06) and $Zn(TFSI)_2$/MIMTFSI-4 (0.12). This high $t_{Zn^{2+}}$ is likely due to the optimized coordination structure of Zn^{2+} facilitated by the fluorinated side chain in the imidazole-based cation, which promotes the release of more free Zn^{2+} ions by disrupting the contact ion pairs of Zn^{2+} and $TFSI^-$.[29]

Molecule dynamics (MD) simulations were conducted to further verify interactions between the ILs and $Zn(TFSI)_2$, as well as ion transport in the $Zn(TFSI)_2$/ILs electrolytes. First, the radial distribution functions (RDFs) highlight a noticeable Zn–F coordination (F from the side chain of MIMTFSI) in $Zn(TFSI)_2$/MIMTFSI-10 compared to the other two electrolytes, suggesting that Zn^{2+} is more closely coordinated with the fluorinated side chain as the chain lengthens (Fig. 2d). The number of $TFSI^-$ ions coordinated with Zn^{2+} also decreases with increasing chain length (Fig. S6, ESI†), indicating that the coordination between the fluorinated side chain and Zn^{2+} can inhibit the formation of a contact ion pair structure between Zn^{2+} and $TFSI^-$. Then, we calculated the diffusion coefficient of Zn^{2+} ion in the three $Zn(TFSI)_2$/ILs electrolytes. Fig. 2e shows that the Zn^{2+} ion in $Zn(TFSI)_2$/MIMTFSI-10 exhibits the highest diffusion coefficient (8.3×10^{-7} cm^2 s^{-1}), likely due to the accelerated Zn^{2+} ion conduction facilitated by the coordination with the fluorinated side chain. Additionally, we examined the binding energy of Zn^{2+} ions with different counterparts to verify the stability of the potential solvation structure. As depicted in Fig. 2f and Fig. S7 (ESI†), the Zn^{2+} ion coordinated with the fluorinated imidazole cation exhibits higher binding energy compared to $Zn^{2+}/TFSI^-$ ion pairs, indicating a strong coordination effect between the fluorinated side chain and Zn^{2+} in $Zn(TFSI)_2$/MIMTFSI-10.

Fabricated SPEs using IL plasticizers

The fabrication of SPE membranes involved incorporating ILs plasticizers into the poly(vinylidene fluoride-*co*-hexafluoropropylene) (PVHF) polymer matrix for its desirable characteristics such as low crystallinity, high ionic conductivity and superior mechanical stability (see the detailed fabrication

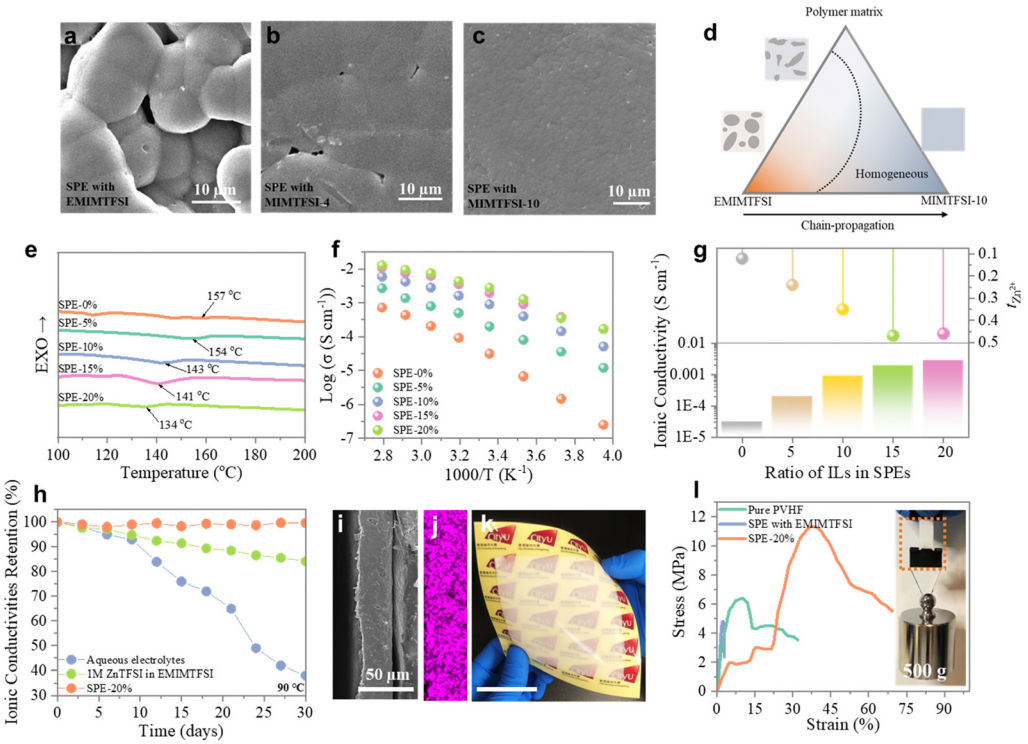

Fig. 3 Fabrication and characteristics of SPEs with IL plasticizers. SEM images of SPEs with different plasticizers at 10% content: (a) EMIMTFSI, (b) MIMTFSI-4, and (c) MIMTFSI-10; (d) the effect of side chains on the compatibility between IL-based plasticizers and the polymer matrix; SPEs with different contents of $Zn(TFSI)_2$/MIMTFSI-10 plasticizers: (e) DSC test, (f) ionic conductivity measurement, (g) $t_{Zn^{2+}}$ measurement; (h) isothermal ionic conductivity of the fabricated SPEs-20%, aqueous electrolytes, and IL electrolyte as a function of time; (i) cross-sectional SEM image of the SPE-20% membrane; (j) Zn elemental mapping of the SPE-20% membrane; (k) optical picture of the large-scale SPE-20% membrane (scale bar: 5 cm); (l) strain–stress curves of the pure PVHF-based SPE and the SPE with IL-based plasticizers (inset picture: load-bearing demonstration of the SPE with the MIMTFSI-10 plasticizer).

Open Access Article. Published on 20 February 2025. Downloaded on 5/22/2025 12:07:16 AM.
This article is licensed under a Creative Commons Attribution-NonCommercial 3.0 Unported Licence.

process in the ESI†).[30] As illustrated in Fig. 3a–c, the EMIMTFSI-based SPE (with 10% content of ILs plasticizer) exhibits severe phase separation, which is diminished in the F-IL-based counterparts. Notably, the MIMTFSI-10-based SPE displays a smooth surface without apparent voids or phase separation, indicating excellent compatibility between the MIMTFSI-10 plasticizer and the polymer matrix. This result suggests the feasibility of extending the side chain to improve compatibility between organic IL plasticizers and polymers (Fig. 3d).

We then investigated the phase behavior of the MIMTFSI-10-based SPEs, denoted as SPE-X, with X representing the weight ratio of MIMTFSI-10-based plasticizers to the polymer matrix, ranging from 0% to 20%. As expected, the inclusion of MIMTFSI-10 plasticizers leads to a gradual decrease in T_m of the SPEs (Fig. 3e). It is worth noting that even with a high plasticizer content of 20%, the SPE still maintains a high T_m of 134 °C, assuring its potential applications in high-temperature scenarios. Thermogravimetric analysis (TGA) curves of the SPEs in Fig. S8 (ESI†) indicate that MIMTFSI-10 plasticizers have minimal influence on the decomposition temperature (T_d) of the SPEs, which remains around 302 °C. This can be attributed to the inherent stability of ILs and excellent compatibility between ILs and the polymer matrix. Such great thermal stability of the SPEs can be promising for constructing high-performance solid zinc batteries that can withstand high-temperature environments. The ionic conductivity of the fabricated SPEs was successively studied, which shows a gradual increase with the addition of the plasticizers (Fig. 3f), reaching a maximum of 2.8×10^{-3} S cm^{-1} (25 °C) for SPE-20%. In addition, SPE-20% demonstrates a notable $t_{Zn^{2+}}$ of 0.46 (Fig. 3g), superior to that of most Zn-based SPEs. These results verify the superiority of the ILs with fluorinated side chains in promoting the Zn^{2+} ion transport, facilitated by the enhanced motion of the side chains and improved compatibility between the polymer matrix and plasticizers. Significantly, the MIMTFSI-10-based SPE can maintain a stable ionic conductivity over an extended period of 30 days at a high temperature of 90 °C, in stark contrast to the rapid decline in ionic conductivity of the aqueous electrolyte and IL electrolyte (Fig. 3h). Furthermore, the MIMTFSI-10-based SPE shows a thickness of 27.5 μm, which is sufficiently thin for applications in flexible devices (Fig. 3i). The uniform dispersion of the Zn element depicted in Fig. 3j further supports the improved compatibility between ILs and the polymer matrix. Moreover, as shown in Fig. 3k, the prepared SPE also shows promising potential for large-scale energy applications.

In addition to its high ionic conductivity and superior thermal stability, the MIMTFSI-10-based SPE also benefits from the excellent fire retardancy properties of ILs, showing improved flame retardancy performance compared to the pure PVHF-based SPE (Fig. S9 and S10, ESI†).[31] This enhancement in flame retardancy can potentially enhance the safety of batteries. Moreover, the inclusion of IL plasticizers leads to improved tensile performance of the MIMTFSI-10-based SPE, as evidenced by the significant increase in the elongation (67%) and the ability to withstand high stress up to 11 MPa (Fig. 3l). The remarkable load-bearing performance of the MIMTFSI-10-based SPE is illustrated in the inset picture of Fig. 3l. These results confirm the high safety and reliability of the fabricated SPEs for energy storage applications.

Reversible Zn anode at elevated temperatures

A Zn‖Ti asymmetric cell was conducted using the prepared SPE to assess the stability and reversibility of the Zn anode. First, cyclic voltammetry (CV) measurements were performed to analyze the Zn plating/stripping behaviors. The results reveal a deposition onset potential (Zn^{2+} to Zn) of −0.068 V *vs.* Zn^{2+}/Zn and a dissolution potential (Zn to Zn^{2+}) of 0.19 V *vs.* Zn^{2+}/Zn (Fig. S11, ESI†). In order to evaluate the potential of the prepared SPE for high-temperature batteries, the reversibility of Zn plating/stripping was further examined at 60 °C and 90 °C. As depicted in Fig. 4a and b, the coulombic efficiency (CE) gradually increases in the initial cycles and maintains values of 99.6% (at 60 °C) and 99.1% (at 90 °C) during the following cycles, demonstrating significant superiority compared to batteries utilizing common aqueous electrolytes and IL electrolytes. Noticeable side reactions, including gassing and decomposition of the aqueous and IL electrolytes, occur during cycling at 90 °C; however, the SPE-based battery exhibits stable Zn plating/stripping behavior with a polarization voltage of 106 mV at an areal current density of 1 mA cm^{-2} (Fig. 4c). In addition, after cycling at 90 °C, the coin cells using aqueous and IL electrolytes exhibited noticeable swelling, whereas the coin cell with the SPE remained unchanged (Fig. S12, ESI†), further confirming the excellent stability of the developed IL-based SPE at high temperatures. Such remarkable performance can be attributed to the fast Zn^{2+} ion transport in the thermally more stable SPE, which ensures stable and highly efficient zinc deposition/dissolution even at high temperatures.

Zn‖Zn symmetric cells were subsequently fabricated for long-term cycling tests. As shown in Fig. S13 (ESI†), stable plating/stripping cycling for up to 2000 h is achieved at 1 mA cm^{-2}, and 1 mA h cm^{-2} at 25 °C. Significantly, the Zn‖Zn symmetric cells exhibit stable plating/stripping even at elevated temperatures, with a cycling life of 1500 h at 60 °C and 800 h at 90 °C, respectively (Fig. 4d and e). It is worth noting that the interfacial resistivity (R_i) of the Zn‖Zn cell retains a reasonable value from 210 Ω to 160 Ω during cycling at 90 °C (Fig. 4f), corroborating the genuine stability of the Zn anode (rather than forming "soft shorts").[32] The dense and dendrite-free surface morphology of the Zn anode indicates complete elimination of Zn dendrites by implementing the prepared SPE (Fig. 4g).[33] Furthermore, we also verified the cycling performance of the Zn‖Zn symmetric cell at a higher depth of discharge (DOD, ~34.2%), which is shown in Fig. S14 (ESI†). The battery can exhibit over 500 h stable cycling, further confirming the advance of the developed F-IL SPEs in delivering highly stable Zn deposition. We also compared the performance of our SPEs with other reports, and the F-IL based SPEs are superior to other solid systems (Table S1, ESI†). Such good performance can be attributed to the high thermal stability and remarkable ion transport kinetics of the developed SPE. Additionally, the electrochemical stability window of the prepared SPE at different temperatures was measured by linear sweep voltammetry (LSV) (Fig. 4h). Despite the slight voltage decrease with increasing temperature, which is likely due to the enhanced electrochemical activity of the polymer chains

 This journal is © The Royal Society of Chemistry 2025

Open Access Article. Published on 20 February 2025 12:07:16 AM.
This article is licensed under a Creative Commons Attribution-NonCommercial 3.0 Unported Licence.

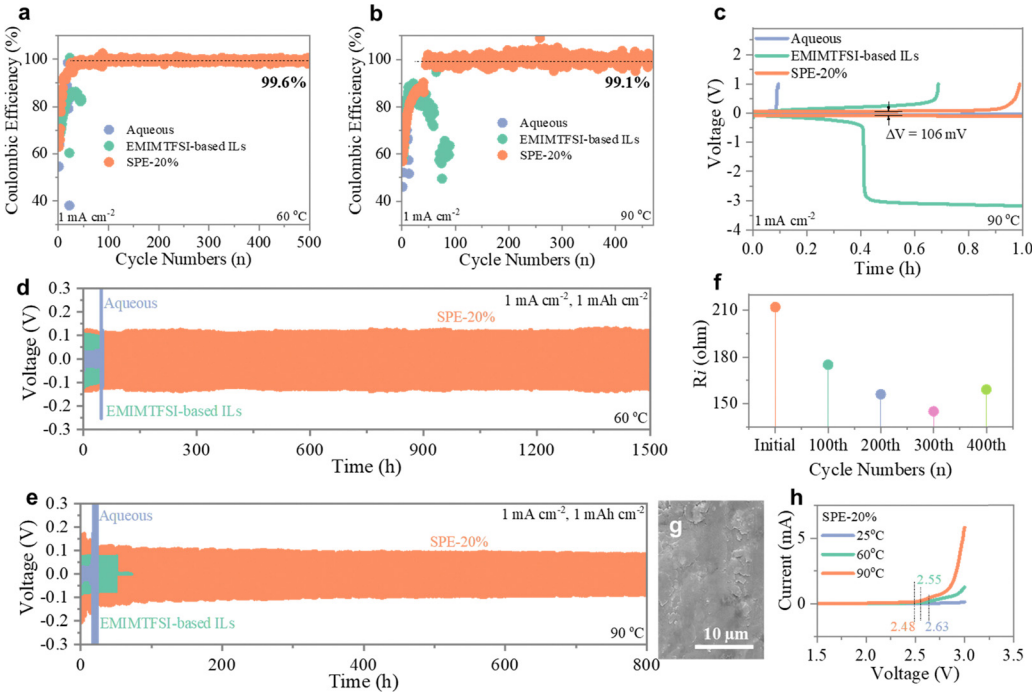

Fig. 4 Reversibility of the Zn anode at elevated temperatures. Zn‖Ti cells with different electrolytes: (a) cycling performance at 60 °C; (b) cycling performance at 90 °C; (c) GCD curves at 90 °C. Zn‖Zn cells with different electrolytes: (d) cycling performance at 60 °C; (e) cycling performance at 90 °C; (f) R_i of the Zn‖Zn cell during cycling at 90 °C; (g) SEM image of the Zn anode after cycling at 90 °C. (h) LSV curves of Zn‖Ti cells based on the prepared SPE at 25 °C, 60 °C, and 90 °C.

at higher temperatures, a wide voltage window of up to 2.48 V (*vs.* Zn^{2+}/Zn) is obtained at 90 °C, superior to common aqueous electrolytes.[34–36] Therefore, our developed SPE greatly contributes to the high reversibility and stability of Zn anodes even under high-temperature conditions, surpassing other reported SPEs.[37–39]

Wide-temperature solid Zn‖Cl4Q full cells

Solid Zn‖Cl4Q batteries were assembled using the optimized F-IL-based SPE regarding its superior ionic conductivity and $t_{Zn^{2+}}$, and excellent thermal stability at elevated temperatures. A typical wide redox peak pair at 1.26/0.83 V is observed in the CV curves of the full cell (Fig. S15, ESI†), corresponding to the redox behavior of the carbonyl groups in Cl4Q.[40] The well-aligned CV curves in subsequent cycles suggest considerable cycling stability of the solid Zn‖Cl4Q battery. To evaluate the potential of this solid ZIB in a wide-temperature power supply, we examined GCD curves at temperatures ranging from −15 °C to 120 °C (Fig. 5a). The polarization voltage between charge and discharge curves gradually decreases with increasing temperature, likely attributed to the enhanced redox activity of active materials and improved Zn^{2+} ion transport kinetics at higher temperatures. Long and flat discharge plateaus are probed over the wide temperature range, indicating decent Zn^{2+} mobility in the solid ZIB facilitated by the advanced F-IL-based plasticizer.[16] Notably, in addition to the high capacity (175 mA h g^{-1}) at elevated temperatures up to 120 °C (Fig. 5b), the solid battery can work effectively even at −15 °C along with a flat discharge plateau and a discharge capacity of 77 mA h g^{-1}, demonstrating its remarkable resistance to heat and freezing. Furthermore, benefiting from the superior thermal and chemical stability of the prepared SPEs, the solid battery achieves a high and stable CE (average value of 99.1%) during cycling in a wide temperature range of −15 to 120 °C, in contrast to the rapidly declining CE of aqueous electrolyte-based and IL electrolyte-based counterparts at elevated temperatures (Fig. 5c). As shown in Fig. 5d, our battery outperforms other electrolyte-based ZIBs, particularly in high-temperature scenarios, exhibiting the widest working temperature window.[41–49] Additionally, the solid Zn‖Cl4Q batteries demonstrate exceptional long-term cycling performance in a wide temperature range (−15 °C to 120 °C) (Fig. 5e and Fig. S16, ESI†), with a remarkable cycling life of 2000 cycles and high capacity retentions of 76.2% (60 °C) and 70.9% (90 °C), respectively. Such significant durability is credited to the excellent stability of the prepared SPE, which shows great competitiveness to other reports (Table S2, ESI†). These findings highlight the effectiveness of our developed SPE in offering solid ZIBs with decent capacity, remarkable wide-temperature electrochemical stability, and cycling durability.

Finally, we fabricated a solid pouch cell with a high Cl4Q loading mass (14 mg cm^{-2}) to further exploit the potential manufacture of the solid Zn‖Cl4Q battery. As shown in Fig. 5f, the solid pouch cell delivers an initial discharge capacity of 82 mA h and maintains a high capacity retention of 79.8% after 500 cycles at 60 °C, suggesting its promising capabilities for large-capacity energy storage. To further investigate the long-term electrochemical performance of the solid Zn‖Cl4Q battery, we conducted tests at 60 °C with different resting times, with measurements taken every 2 days over the course of three months. As illustrated in Fig. 5g, the solid battery delivers similar discharge

Open Access Article. Published on 20 February 2025. Downloaded on 5/22/2025 12:07:16 AM.
This article is licensed under a Creative Commons Attribution-NonCommercial 3.0 Unported Licence.

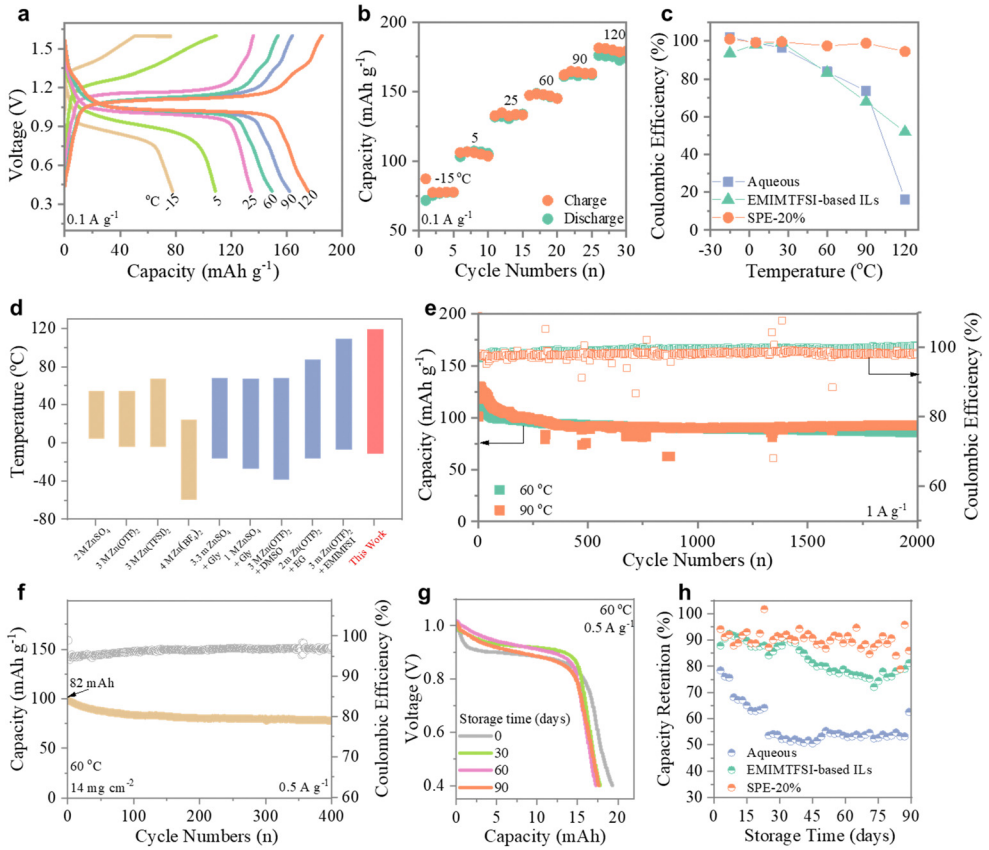

Fig. 5 Electrochemical performance of solid Zn‖Cl4Q full cells. Solid Zn‖Cl4Q full cells measured at temperatures ranging from −15 °C to 120 °C: (a) GCD curves; (b) charging/discharging capacity; (c) CE of the solid battery and its counterparts based on aqueous and IL electrolytes. (d) Comparison of the working temperature window in our SPE-based ZIB and other reported ZIBs;[41–49] (e) long-term cycling performance of the solid Zn‖Cl4Q battery at 60 °C and 90 °C; (f) cycling performance of the solid pouch cell with a high loading mass of Cl4Q; (g) GCD curves of the solid battery after different resting times; (h) the capacity retention of the solid battery and its counterparts based on aqueous and IL electrolytes. Gly: glycine, EG: ethylene glycol, and DMSO: dimethyl sulfoxide.

curves and retains approximately 91.2% of its initial discharge capacity even after resting for 90 days, showcasing an exceptionally low self-discharge rate (average capacity loss of 0.09% per day). The solid battery demonstrates significantly higher capacity retention than its counterparts based on aqueous and IL electrolytes, highlighting the solid system's outstanding shelf life and high reliability (Fig. 5h). These results underscore the excellent anti-self-discharge capability and temperature adaptability of the F-IL-based SPE, which holds tremendous promise for the development of highly stable and durable solid ZIBs for practical applications.

Conclusions

Incorporating IL plasticizers in SPEs is promising for improving their ionic conductivity, which is crucial for the fabrication of high-performance ZIBs. However, the strong Zn^{2+}-anion interactions restrict $t_{Zn^{2+}}$ of IL-based SPEs and the poor compatibility between ILs and the polymer matrix results in serious phase separation. In this study, we designed F-ILs with extended fluorinated side chains to release more free Zn^{2+} ions by modifying the Zn^{2+} solvation structure and simultaneously enhancing the compatibility between ILs and the polymer matrix. Benefiting from the high ionic conductivity, notable $t_{Zn^{2+}}$, and excellent thermal stability of the developed SPEs, long-term stable Zn plating/stripping without Zn dendrites or the HER was achieved. Furthermore, the solid Zn‖Cl4Q battery delivered remarkable electrochemical performance across a wide working temperature window (from −15 °C to 120 °C), surpassing other reported solid ZIBs. The pouch cell demonstrated an excellent shelf life of 90 days and a low self-discharge rate (average capacity loss of 0.09% per day) at 60 °C. This work shed new light on the design of Zn^{2+}-based SPEs, significantly advancing high-performance and stable solid ZIBs.

Author contributions

Writing – original draft: Z. C.; writing – review & editing: Z. C. and C. Y. Z.; conceptualization: Z. C., Z. Q. W., Y. Q. W., A. C. and Z. D. H.; investigation: Z. C. and N. L.; methodology: Z. C., T. L. and D. Y. C.; funding acquisition: C. Y. Z.

Data availability

The data supporting this article have been included as part of the ESI.†

 This journal is © The Royal Society of Chemistry 2025

Open Access Article. Published on 20 February 2025. Downloaded on 5/22/2025 12:07:16 AM. This article is licensed under a Creative Commons Attribution-NonCommercial 3.0 Unported Licence.

Conflicts of interest

The authors declare no competing interests.

Acknowledgements

This research was supported by the National Key R&D Program of China under Project 2019YFA0705104. It was supported in part by the InnoHK Project on [Project 1.4 – Flexible and Stretchable Technologies (FAST) for monitoring of CVD risk factors: soft battery and self-powered, flexible medical devices] at Hong Kong Centre for Cerebro-cardiovascular Health Engineering (COCHE).

References

1 M. S. Lavine, *Science*, 2017, **356**, 392.
2 L. Ma, M. A. Schroeder, O. Borodin, T. P. Pollard, M. S. Ding, C. Wang and K. Xu, *Nat. Energy*, 2020, **5**, 743–749.
3 L. Cao, D. Li, T. Pollard, T. Deng, B. Zhang, C. Yang, L. Chen, J. Vatamanu, E. Hu, M. J. Hourwitz, L. Ma, M. Ding, Q. Li, S. Hou, K. Gaskell, J. T. Fourkas, X.-Q. Yang, K. Xu, O. Borodin and C. Wang, *Nat. Nanotechnol.*, 2021, **16**, 902–910.
4 T. Zhang, Y. Tang, S. Guo, X. Cao, A. Pan, G. Fang, J. Zhou and S. Liang, *Energy Environ. Sci.*, 2020, **13**, 4625–4665.
5 B. Tang, L. Shan, S. Liang and J. Zhou, *Energy Environ. Sci.*, 2019, **12**, 3288–3304.
6 X. Jia, C. Liu, Z. G. Neale, J. Yang and G. Cao, *Chem. Rev.*, 2020, **120**, 7795–7866.
7 X. Wu, Y. Xu, C. Zhang, D. P. Leonard, A. Markir, J. Lu and X. Ji, *J. Am. Chem. Soc.*, 2019, **141**, 6338–6344.
8 Y. Yamada, K. Usui, K. Sodeyama, S. Ko, Y. Tateyama and A. Yamada, *Nat. Energy*, 2016, **1**, 16129.
9 Z. Chen, F. Mo, T. Wang, Q. Yang, Z. Huang, D. Wang, G. Liang, A. Chen, Q. Li, Y. Guo, X. Li, J. Fan and C. Zhi, *Energy Environ. Sci.*, 2021, **14**, 2441–2450.
10 S. Zhao, Y. Zuo, T. Liu, S. Zhai, Y. Dai, Z. Guo, Y. Wang, Q. He, L. Xia, C. Zhi, J. Bae, K. Wang and M. Ni, *Adv. Energy Mater.*, 2021, **11**, 2101749.
11 J. Ming, J. Guo, C. Xia, W. Wang and H. N. Alshareef, *Mater. Sci. Eng., R*, 2019, **135**, 58–84.
12 L. Kang, M. Cui, Z. Zhang and F. Jiang, *Batteries Supercaps*, 2020, **3**, 966–1005.
13 G. Fang, J. Zhou, A. Pan and S. Liang, *ACS Energy Lett.*, 2018, **3**, 2480–2501.
14 H. Yang, R. Huq and G. C. Farrington, *Solid State Ionics*, 1990, **40–41**, 663–665.
15 E. J. Hansen and J. Liu, *Front. Energy Res.*, 2021, **8**, 616665.
16 Z. Chen, T. Wang, Y. Hou, Y. Wang, Z. Huang, H. Cui, J. Fan, Z. Pei and C. Zhi, *Adv. Mater.*, 2022, **34**, 2207682.
17 T. Zhou, Y. Zhao, J. W. Choi and A. Coskun, *Angew. Chem., Int. Ed.*, 2021, **60**, 22791–22796.
18 Z. Chen, X. L. Li, D. H. Wang, Q. Yang, L. T. Ma, Z. D. Huang, G. J. Liang, A. Chen, Y. Guo, B. B. Dong, X. Y. Huang, C. Yang and C. Y. Zhi, *Energy Environ. Sci.*, 2021, **14**, 3492–3501.
19 J. Atik, D. Diddens, J. H. Thienenkamp, G. Brunklaus, M. Winter and E. Paillard, *Angew. Chem., Int. Ed.*, 2021, **60**, 11919–11927.
20 D. Ranjith Kumar, P. Muhammed Shafi, R. Karthik, G. Dhakal, S.-H. Kim, M. Kim and J.-J. Shim, *J. Mol. Liq.*, 2022, **367**, 120399.
21 F. Ilyas, M. Ishaq, M. Jabeen, M. Saeed, A. Ihsan and M. Ahmed, *J. Mol. Liq.*, 2021, **343**, 117606.
22 D. Wang, X. Guo, Z. Chen, Y. Zhao, Q. Li and C. Zhi, *ACS Appl. Mater. Interfaces*, 2022, **14**, 27287–27293.
23 Y. Kitazawa, K. Ueno and M. Watanabe, *Chem. Rec.*, 2018, **18**, 391–409.
24 L. Wei, L. Wang, Z. Cui, Y. Liu and A. Du, *Molecules*, 2023, **28**, 3836.
25 X. Ma, J. Yu, Y. Hu, J. Texter and F. Yan, *Ind. Chem. Mater.*, 2023, **1**, 39–59.
26 L. Chen, H. Wu, X. Ai, Y. Cao and Z. Chen, *Battery Energy*, 2022, **1**, 20210006.
27 H. Qiu, X. Du, J. Zhao, Y. Wang, J. Ju, Z. Chen, Z. Hu, D. Yan, X. Zhou and G. Cui, *Nat. Commun.*, 2019, **10**, 1–12.
28 Q. Lu, J. Fu, L. Chen, D. Shang, M. Li, Y. Xu, R. Jia, S. Yuan and L. Shi, *J. Power Sources*, 2019, **414**, 31–40.
29 T. Frömling, M. Kunze, M. Schönhoff, J. Sundermeyer and B. Roling, *J. Phys. Chem. B*, 2008, **112**, 12985–12990.
30 Z. Chen, X. Ma, Y. Hou, H. Cui, X. Li, Q. Yang, Z. Huang, D. Wang, B. Dong, J. Fan and C. Zhi, *Adv. Funct. Mater.*, 2023, **33**, 2214539.
31 K. Liu, Z. Wang, L. Shi, S. Jungsuttiwong and S. Yuan, *J. Energy Chem.*, 2021, **59**, 320–333.
32 Q. Li, A. Chen, D. Wang, Z. Pei and C. Zhi, *Joule*, 2022, **6**, 273–279.
33 X. L. Li, Q. Li, Y. Hou, Q. Yang, Z. Chen, Z. D. Huang, G. J. Liang, Y. W. Zhao, L. T. Ma, M. A. Li, Q. Huang and C. Y. Zhi, *ACS Nano*, 2021, **15**, 14631–14642.
34 Z. Huang, Y. Hou, T. Wang, Y. Zhao, G. Liang, X. Li, Y. Guo, Q. Yang, Z. Chen, Q. Li, L. Ma, J. Fan and C. Zhi, *Nat. Commun.*, 2021, **12**, 3106.
35 Z. Chen, S. Wang, Z. Wei, Y. Wang, Z. Wu, Y. Hou, J. Zhu, Y. Wang, G. Liang, Z. Huang, A. Chen, D. Wang and C. Zhi, *J. Am. Chem. Soc.*, 2023, **145**, 20521–20529.
36 Z. Chen, Y. Hou, Y. Wang, Z. Wei, A. Chen, P. Li, Z. Huang, N. Li and C. Zhi, *Adv. Mater.*, 2023, 2309330.
37 I. M. De Cachinho Cordeiro, A. Li, B. Lin, D. X. Ma, L. Xu, A. L.-S. Eh and W. Wang, *Batteries*, 2023, **9**, 343.
38 S. N. Patel, *ACS Macro Lett.*, 2021, **10**, 141–153.
39 K. Wu, J. Huang, J. Yi, X. Liu, Y. Liu, Y. Wang, J. Zhang and Y. Xia, *Adv. Energy Mater.*, 2020, **10**, 1903977.
40 Q. Zhao, W. Huang, Z. Luo, L. Liu, Y. Lu, Y. Li, L. Li, J. Hu, H. Ma and J. Chen, *Sci. Adv.*, 2018, **4**, eaao1761.
41 L. Yu, J. Huang, S. Wang, L. Qi, S. Wang and C. Chen, *Adv. Mater.*, 2023, **35**, 2210789.
42 Y. Yang, Y. Tang, S. Liang, Z. Wu, G. Fang, X. Cao, C. Wang, T. Lin, A. Pan and J. Zhou, *Nano Energy*, 2019, **61**, 617–625.
43 W. Deng, Z. Zhou, Y. Li, M. Zhang, X. Yuan, J. Hu, Z. Li, C. Li and R. Li, *ACS Nano*, 2020, **14**, 15776–15785.
44 H. Glatz, E. Tervoort and D. Kundu, *ACS Appl. Mater. Interfaces*, 2020, **12**, 3522–3530.
45 B. Tang, J. Zhou, G. Fang, F. Liu, C. Zhu, C. Wang, A. Pan and S. Liang, *J. Mater. Chem. A*, 2019, **7**, 940–945.

Open Access Article. Published on 20 February 2025. Downloaded on 5/22/2025 12:07:16 AM.
This article is licensed under a Creative Commons Attribution-NonCommercial 3.0 Unported Licence.

46 N. Zhang, Y. Dong, M. Jia, X. Bian, Y. Wang, M. Qiu, J. Xu, Y. Liu, L. Jiao and F. Cheng, *ACS Energy Lett.*, 2018, **3**, 1366–1372.
47 T. Sun, X. Yuan, K. Wang, S. Zheng, J. Shi, Q. Zhang, W. Cai, J. Liang and Z. Tao, *J. Mater. Chem. A*, 2021, **9**, 7042–7047.
48 M. Chen, J. Chen, W. Zhou, X. Han, Y. Yao and C.-P. Wong, *Adv. Mater.*, 2021, **33**, 2007559.
49 H. Lu, J. Hu, L. Wang, J. Li, X. Ma, Z. Zhu, H. Li, Y. Zhao, Y. Li, J. Zhao and B. Xu, *Adv. Funct. Mater.*, 2022, **32**, 2112540.

 This journal is © The Royal Society of Chemistry 2025